The 2016 Summer Floods in China and Associated Physical Mechanisms: A Comparison with 1998

Yuan YUAN[1], Hui GAO[1], Weijing LI[1,2*], Yanju LIU[1], Lijuan CHEN[1,2], Bin ZHOU[1], and Yihui DING[1]

1 *Laboratory for Climate Studies*, *National Climate Center*, *China Meteorological Administration*, *Beijing* 100081
2 *Collaborative Innovation Center on Forecast and Evaluation of Meteorological Disasters*, *Nanjing University of Information Science &Technology*, *Nanjing* 210044

(Received October 17, 2016; in final form January 12, 2017)

ABSTRACT

The characteristics of droughts and floods in China during the summers (May–August) of 2016 and 1998 were compared in great detail, together with the associated atmospheric circulations and external-forcing factors. Following results are obtained. (1) The precipitation was mostly above normal in China in summer 2016, with two main rainfall belts located in the Yangtze River valley (YRV) and North China. Compared with 1998, a similar rainfall belt was located over the YRV, with precipitation 100% and more above normal. However, the seasonal processes of Meiyu were different. A typical "Secondary Meiyu" occurred in 1998, whereas dry conditions dominated the YRV in 2016. (2) During May–July 2016, the Ural high was weaker than normal, but it was stronger than normal in 1998. This difference resulted from fairly different distributions of sea surface temperature anomalies (SSTAs) over the North Atlantic Ocean during the preceding winter and spring of the two years. (3) Nonetheless, tropical and subtropical circulation systems were much more similar in May–July of 2016 and 1998. The circulation systems in both years were characterized by a stronger than normal and more westward-extending western Pacific subtropical high (WPSH), a weaker than normal East Asian summer monsoon (EASM), and anomalous convergence of moisture flux in the mid and lower reaches of the YRV. These similar circulation anomalies were attributed to the similar tropical SSTA pattern in the preceding seasons, i.e., the super El Niño and strong warming in the tropical Indian Ocean. (4) Significant differences in the circulation pattern were observed in August between the two years. The WPSH broke up in August 2016, with its western part being combined with the continental high and persistently dominating eastern China. The EASM suddenly became stronger, and dry conditions prevailed in the YRV. On the contrary, the EASM was weaker in August 1998 and the "Secondary Meiyu" took place in the YRV. The Madden–Julian Oscillation (MJO) was extremely active in August 2016 and stayed in western Pacific for 25 days. It triggered frequent tropical cyclone activities and further influenced the significant turning of tropical and subtropical circulations in August 2016. In contrast, the MJO was active over the tropical Indian Ocean in August 1998, conducive to the maintenance of a strong WPSH. Alongside the above oceanic factors and atmospheric circulation anomalies, the thermal effect of snow cover over the Qinghai–Tibetan Plateau from the preceding winter to spring in 2016 was much weaker than that in 1998. This may explain the relatively stronger EASM and more abundant precipitation in North China in 2016 than those in 1998.

Key words: summer precipitation, flooding, Yangtze River valley, super El Niño, SST anomaly, tropical Indian Ocean, snow cover over the Qinghai–Tibetan Plateau, Madden–Julian Oscillation

Citation: Yuan, Y., H. Gao, W. J. Li, et al., 2017: The 2016 summer floods in China and associated physical mechanisms: A comparison with 1998. *J. Meteor. Res.*, **31**(2), 261–277, doi: 10.1007/s13351-017-6192-5.

1. Introduction

Located in the Asian–Australian monsoon region, the climate of China is deeply affected by the thermal conditions of the Qinghai–Tibetan Plateau (QTP), the SST in the Indian Ocean and Pacific Ocean, and the circulation systems of the Asian summer monsoon. Owing to its complex factors of influence, China experiences the most drought and flood events in the world. According to the statistics, the economic losses caused by meteorological

Supported by the National (Key) Basic Research and Development (973) Program of China (2013CB430203), China Meteorological Administration Special Public Welfare Research Fund (GYHY201306033 and GYHY201406001), and National Natural Science Foundation of China (41130960).

*Corresponding author: liwj@cma.gov.cn.

disasters account for about 71% of the total losses by natural disasters, and 80% of them are induced by drought and flood disasters (Li et al., 2009). In China, floods occur mainly in the second half of the year owing to the monsoonal climate at this time, especially during the summer season (May–August in this paper; MJJA for short). Severe floods exert huge negative impacts on the lives of the people and the economic development of China. For example, in 1991, the number of deaths caused by severe floods in the Yangtze River valley (YRV) was around 1200, and the direct economic loss was over 10 billion US dollars. Even worse, the extreme floods in 1998 caused 3004 deaths and an estimated economic loss of nearly 25 billion RMB [National Climate Center (NCC), 1998].

As the most important system influencing global climate, the occurrence and development of the El Niño–Southern Oscillation (ENSO) has significant impacts on the East Asian summer monsoon (EASM) and causes drought or flood disasters in some regions. During 1997–98, a super El Niño event occurred in the equatorial eastern Pacific. Both the cumulative intensity and the peak intensity exceeded those of a previous super El Niño event in 1982/83. Many studies have revealed the influences of the 1997/98 El Niño on the extreme floods of the YRV, as well as the severe floods in Nenjiang and Songhua River in Northeast China during the summer of 1998. The potential application of ENSO in seasonal forecasting has also been discussed in many studies (NCC, 1998; Li, 1999; Chen, 2001; Wang et al., 2012). Since the turn of the 21st century, ENSO events have become weaker, and studies have explored the notion that moderate or weak ENSO events can be modulated by other factors (Xue and Liu, 2008; Liu and Xue, 2010). However, the influences of strong ENSO events on the EASM and on summer precipitation in China cannot be ignored in seasonal climate forecasts (Zhao, 1999; Chen and Zhao, 2000). During 2014–16, a super El Niño event occurred again in the equatorial central–eastern Pacific. The event reached its peak in November 2015. Its maximal intensity even exceeded that of the 1982/83 and 1997/98 events (Shao and Zhou, 2016; Yuan et al., 2016; Zhai et al., 2016). Affected by this event, the summer precipitation in 2016 in the YRV was much higher than normal, and severe floods occurred in the mid and lower reaches of the river. In March 2016, the NCC successfully predicted the floods in this region.

Besides ENSO, the SST anomaly (SSTA) in the tropical Indian Ocean (TIO) can also affect the summer monsoon and precipitation anomaly in China (Chen et al., 2013). Before the discovery of the tropical Indian Ocean dipole (IOD; Saji et al., 1999), Luo et al. (1985) revealed that the previous SSTA in the Arabian Sea and southern Bay of Bengal correlates well with the summer precipitation over the mid and lower reaches of the YRV. When the IOD index is positive, less precipitation occurs over North China and the Huai River basin, while South China tends to be wetter than normal, especially along its coast. Additionally, the Indian Ocean basin-wide mode (IOBW) is the most important mode of SSTA in the TIO. It usually develops in winter and reaches its peak in the following spring. Connected by the "atmospheric bridge" or the Indonesian throughflow, the SST in the TIO tends to be warmer (colder) from winter to the following summer after an El Niño (or a La Niña) event (Meyers, 1996; Klein et al., 1999; Lau and Nath, 2000). During the process, the Indian Ocean acts as a capacitor to prolong ENSO's impact on East Asia (Yang et al., 2007; Xie et al., 2009). When the TIO is warmer than normal, the summer precipitation over the YRV tends to be more abundant (Hu K. M. et al., 2011).

The factors affecting precipitation in China are quite complex and diverse. Besides global SSTs, land-surface thermal processes, such as the Arctic sea ice and snow cover over the QTP or over Eurasian continent, can also influence the position and intensity of the summer rainfall belt in the country. Among these factors, the area of snow cover over the QTP in the previous winter and spring is thought to play a key role (Zhao, 1999; Chen and Zhao, 2000). Statistical results show that both the western Pacific subtropical high (WPSH) and the main rainfall belt in China tend to be situated more southwards in summer after a larger area of snow cover in the QTP during the previous winter, and vice versa. For the winter of 1997/98, the abnormally larger snow cover over the QTP has been considered as one of the most important seasonal forecast signals for the persistent flood event in the YRV during the summer of 1998 (Li, 1999).

However, the influences of ENSO events, SSTAs in the TIO, and the snow cover over the QTP, are primarily limited to the tropical–subtropical regions of East Asia. The position and intensity of the summer rainfall belt depend not only on the warm and wet flow from the tropical ocean, but also on the cold and dry air from the high latitudes. Therefore, the circulation anomalies at high latitudes and the associated external-forcing signals are also important for the seasonal forecasting of summer precipitation. Analyses of both observational diagnoses and numerical simulations show that the SSTA in the North Atlantic Ocean can affect the interannual variability of the EASM by stimulating a zonal teleconnection wave pat-

tern across the Eurasian continent (Wu et al., 2009; Zuo et al., 2012). In the winter of 1997/98, the SSTA in the North Atlantic Ocean showed a strong negative phase of triple mode from the tropics to the high latitudes, which led to more frequent blocking activities in the following summer and caused a WPSH that was situated more southward, especially in July. That was also one of the main reasons for the extreme flood along the YRV in the summer of 1998 (NCC, 1998).

The present study focuses on three questions: (1) What are the differences and similarities of the summer precipitation between 2016 and 1998? (2) What are the differences of the precursor signals between 2016 and 1998? (3) How do these precursor signals influence the summer precipitation in China in 2016?

2. Data and method

The observed daily rainfall amounts at over 2000 Chinese meteorological stations were provided by the China Meteorological Administration. For data quality, only those stations with complete data during 1981–2016 were selected for further study (Ren et al., 2012). The atmospheric variables were obtained from the NCEP–NCAR reanalysis (Kalnay et al., 1996; Kistler et al., 2001), including 500-hPa geopotential height, 850-hPa horizontal wind, relative humidity, and so on. These data have a 2.5° × 2.5° (latitude × longitude) resolution. The monthly SST data were obtained from the OISST v2 (Optimum Interpolation Sea Surface Temperature, version 2) dataset of the NOAA, with a 1° × 1° (latitude × longitude) resolution (Reynolds et al., 2002). The area of snow cover in the Northern Hemisphere was derived from NOAA satellite monitoring data. Snow depth data for China since 9 July 1987 were corrected by inversion from station observations (Chang et al., 1976, 1982; Che and Li, 2005). According to the standard of the WMO, the climate normal is the average of a climatological variable over the latest three decades, i.e., 1981–2010. Therefore, the anomalies of all variables were derived based on the climate mean of 1981–2010, except the data from OISST v2 (climate normal period was 1982–2010) and the microwave snow depth data (1990–2009). In this paper, boreal winter refers to the three-month mean of December–February, whilst spring refers to the March–May mean, summer to the June–August mean, and autumn to the September–November mean.

Furthermore, the South China Sea summer monsoon (SCSSM) onset date is defined as the first pentad when the averaged 850-hPa zonal wind is stably positive in the South China Sea (10°–20°N, 110°–120°E) region, and the area-averaged mean pseudo-equivalent temperature is also stably greater than 340 K at the same time. The EASM index is defined as the differences of 850-hPa zonal wind between the tropical monsoon trough region (10°–20°N, 100°–150°E) and the East Asian subtropical monsoon region (25°–35°N, 100°– 150°E) (Zhang et al., 2003). The WPSH intensity data were obtained from Liu et al. (2012). According to the National Meiyu Monitoring Standard of China, the Meiyu amount is the accumulated precipitation from its beginning day to its end day. Based on Wang and Zhang (2002), the Philippine Sea anticyclone index (PSAC) is defined as the mean sea level pressure in northwestern Pacific (0°–20°N, 110°–140°E). The tropical IOBW index is defined as the area-averaged SSTA in the TIO (20°S–20°N, 40°–110°E). The tropical IOD index is defined as the SSTA difference between the western Indian Ocean (10°S–10°N, 50°–70°E) and the southeastern Indian Ocean (0°–10°S, 90°–110°E; Saji et al., 1999). The Niño3.4 index is defined as the averaged SSTA in the Niño3.4 region (5°S–5°N, 170°–120°W). The North Atlantic Triple (NAT) index is defined as the time series of the first EOF mode of the SSTA in the North Atlantic Ocean (0°–60°N, 80°W–0°). A positive (negative) NAT phase corresponds to a "– + –" ("+ – +") pattern of SSTA from low to high latitudes. The daily Madden–Julian Oscillation (MJO) index was obtained from the Australian Bureau of Meteorology (http://www.bom.gov.au/climate/mjo/) by Wheeler and Hendon (2004).

3. Comparison of summer precipitation

3.1 *Monthly and seasonal precipitation features*

In MJJA 2016, the precipitation was above normal in most areas of China (Fig. 1a). The area-averaged precipitation over the whole country was 8% above normal and ranked the fourth highest value since 1951, which was less than that in 1998 (22%) and 1954 (26%). The spatial pattern of the precipitation anomaly in southern China was similar to that in 1998 (Fig. 1b), with the main rainfall belt located in the mid and lower reaches of the YRV. However, the extreme floods occurred throughout the whole YRV in 1998, with a larger area and stronger intensity than in 2016.

The precipitation pattern was quite different in northern China between the two years. In 2016, the precipitation was about 20%–50% below normal in eastern Inner Mongolia, but it was 50%–80% above normal in 1998. In 2016, the precipitation was less than normal in the eastern part of Northwest China and the Huanghuai area, but

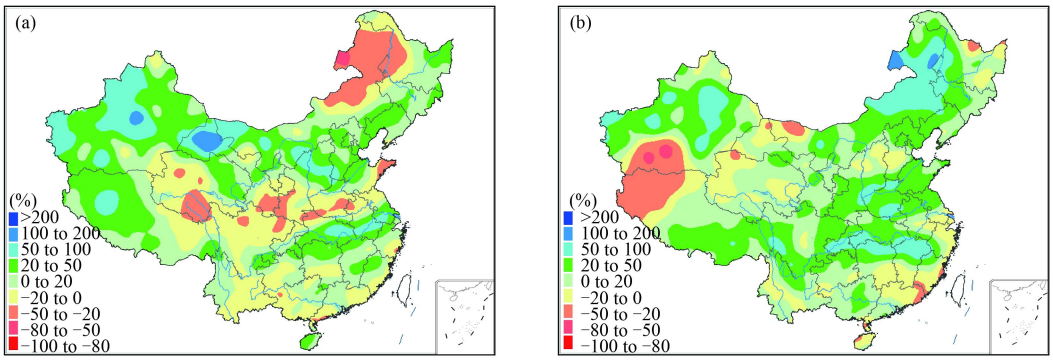

Fig. 1. Percentage anomalies of precipitation averaged in May–August of (a) 2016 and (b) 1998.

was more than normal in 1998. Opposite anomalies could also be found in North China and Northeast China. In 1998, severe floods occurred both in Nenjiang and the Songhua River. In 2016, however, the precipitation in Northeast China was much less than that in 1998, and moderate drought even occurred in July and August. In summer 2016, there were two centers with a greater than 50% anomaly of precipitation in China—one in the YRV and the other in North China. Such a summer rainfall pattern has been extremely rare since 1951.

Intraseasonal differences are also quite obvious between the two years. In May 2016, more precipitation occurred mainly over the lower reaches of the YRV, Huai River, and eastern Northeast China. In June and July, above-normal rainfall dominated over the mid and lower reaches of the YRV and northern China. During that period, the extreme rainstorm event of 18–21 July made a considerable contribution to the whole flood season in North China. In August, except parts of southern China where there was more precipitation, the precipitation in most regions of eastern China was below normal. In the YRV in particular, the precipitation was 50%–80% less than normal. It can be seen that a pronounced intraseasonal inversion of summer precipitation occurred in August 2016, with the main rainfall belt in the YRV and North China during May–July (MJJ) and dry conditions in August. In 1998, however, this intraseasonal turning occurred around June. In May, more precipitation dominated in the northern regions of the YRV. In June–August, however, the major rainfall belt persisted mainly in the YRV and Northeast China. For convenience, the summer rainy seasons of 2016 and 1998 are divided into two periods (MJJ and August) for further investigation. It can be seen that the precipitation anomaly pattern in MJJ 2016 (Fig. 2a) was quite similar to the pattern in MJJA 2016 (Fig. 1a), whereas the pattern in August (Fig. 2b) was almost opposite. In 1998, the patterns both in MJJ (Fig. 2c) and in August (Fig. 2d) were similar to that for the whole rainy season (Fig. 1b).

3.2 *Seasonal progression and extreme features of precipitation*

Obvious differences also existed in the seasonal progression of precipitation in eastern China between the two years. During May to mid-June of 2016, the major rainfall belt was located in the mid and lower reaches of the YRV and its southern area, which was more northward than the rainfall belt in the same period of 1998. In mid-June 2016, the atmospheric circulation began to adjust and the ridge line of the WPSH moved to the north of 20°N. As a result, the main rainfall belt also moved northward to 30°–35°N. Therefore, the Chinese Meiyu over the YRV began on 19 June 2016, which was 5 days later than normal. During the Meiyu period, the most severe flooding occurred from 28 June to 6 July, and the heavy rainstorm influenced at least 451 national meteorological stations in China. The intensity of this heavy rain process ranked the fifth strongest for a single case since 1961. From 18 to 21 July, an extreme heavy rainfall event occurred in North China. In August, the major rainfall belt withdrew southward, and dry and hot weather appeared over the river and its northern region (Fig. 3a).

However, the rainfall progression in 1998 was quite different. In that year, the rainfall belt advanced from South China to North China during early and middle summer. From May to early June, the ridge line of the WPSH was located at 15°N (figure omitted). Corresponding to this pattern, the major rainfall belt lay in southern China. From mid-June to early July, the WPSH jumped to 20°N. Affected by the shift, the Meiyu over the YRV began on 11 June, and the Meiyu over the Huai River began on 25 June. The WPSH jumped northward again to 25°N in mid-July. As a result, the rainy season in the YRV was interrupted and the major rainfall belt reached the Huanghuai River basin and North China. However, the WPSH retreated southward on 17 July

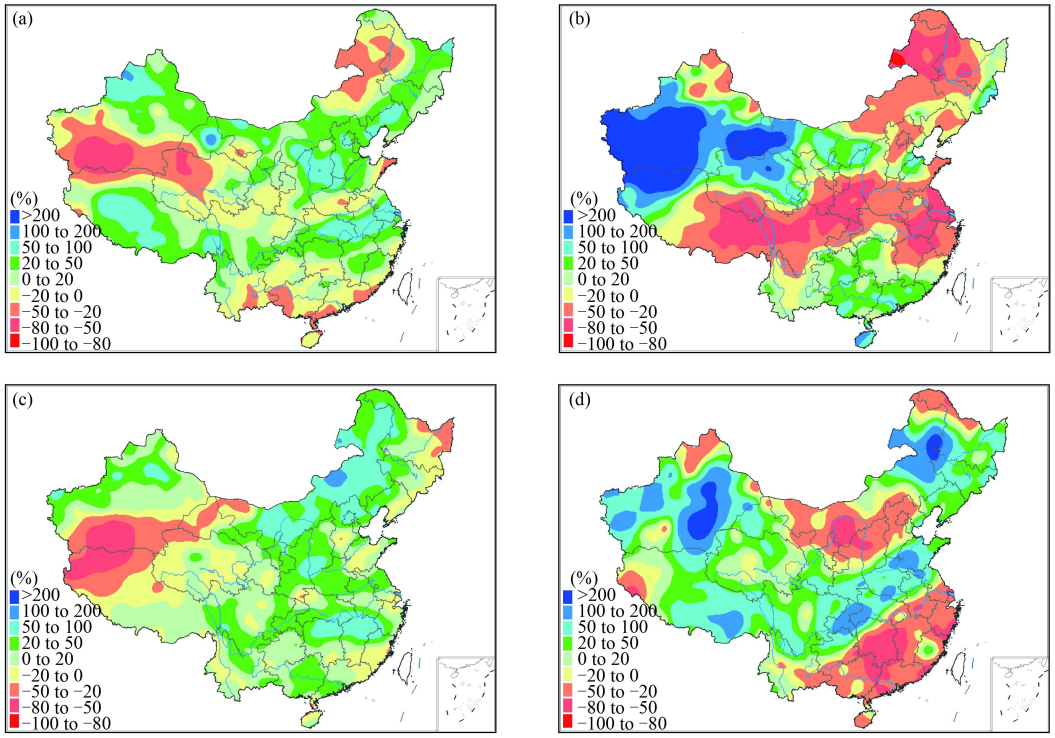

Fig. 2. Percentage anomalies of precipitation in (a, c) MJJ and (b, d) August of (a, b) 2016 and (c, d) 1998.

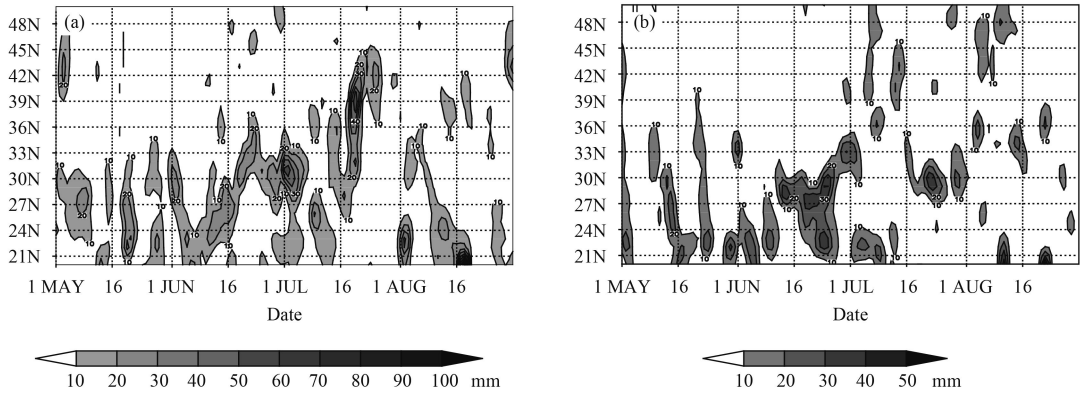

Fig. 3. Time–latitude cross-sections of daily precipitation amount (mm) in eastern China (to the east of 110°E) in (a) 2016 and (b) 1998.

1998. The Yangtze River thereby experienced heavy rainstorms again. The rainstorm during this period was shorter than the previous one, but was much stronger (NCC, 1998), and thereby became a typical "Secondary Meiyu" in the YRV (Fig. 3b).

Compared with 1998, summer precipitation in North China was obviously more abundant in summer 2016 (Fig. 1b). However, it can be observed that the average rainfall amounts of all the processes in North China were less than 20 mm, except the extreme one during 19–20 July (Fig. 4a). The accumulated precipitation during 19–20 July accounts for 25% of the total rainfall in MJJA 2016, indicating that this process played an important role in the above-normal summer precipitation of North China. In the mid and lower reaches of the YRV (Fig. 4b), the evolutionary features of precipitation were similar before early July in the two years. However, dry conditions occurred from 5 July 1998 and a "Secondary Meiyu" happened again from late July to early August. In 2016, the Meiyu in the YRV ended on 21 July and the precipitation was much less than normal throughout the whole of August. Despite the different evolutions of Meiyu between the two years, the Meiyu amounts were quite similar and both over 100% above normal, with 104% in 1998 and 108% in 2016 (Fig. 5).

From the above analyses, some similarities and differences in the characteristics of summer precipitation between 2016 and 1998 can be concluded. The total pre-

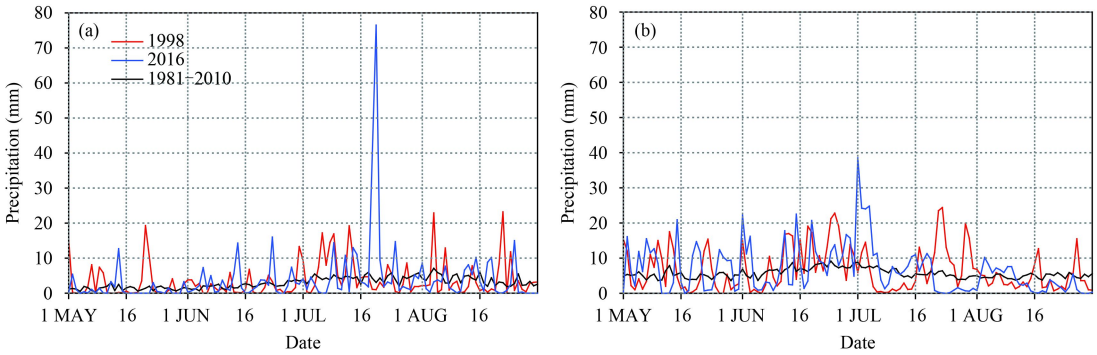

Fig. 4. Daily precipitation amount (mm) averaged over (a) North China and (b) the mid and lower reaches of the Yangtze River in 1998 (red) and 2016 (blue), and the 30-yr mean of 1981–2010 (black).

cipitation in summer was in both cases greater than normal, and both years featured two major rainfall belts in eastern China—one in the YRV and the other over northern China. The Meiyu amounts in the two years were both double the normal value. However, a typical "Secondary Meiyu" event occurred in the Yangtze River region during late July and early August in 1998. In the same period of 2016, however, the Yangtze River experienced high temperatures and extreme dry conditions. In 1998, severe flooding occurred in Northeast China, whereas in 2016 drought happened in eastern Inner Mongolia. Affected by the extreme heavy rainstorm process during 18–21 July, the summer precipitation over North China in 2016 was greater than that in 1998.

4. Atmospheric circulation and monsoon features

Considering the significant turning of the precipitation anomaly in eastern China in August 2016, the circulation anomalies of the MJJ mean and for August are analyzed separately.

4.1 *Anomalies of atmospheric circulation and their developing features*

In MJJ 2016, the meridional gradient of the atmospheric circulation over the mid and high latitudes was smaller than normal, with a weaker Ural high ridge and stronger blocking over the Sea of Okhotsk. Meanwhile, the WPSH was stronger than normal, with its high ridge extending more westward (Fig. 6a). In the lower troposphere, an anomalous anticyclone dominated over northwestern Pacific (Fig. 6c); and there was intensified water vapor transport from the western Pacific to the mid and lower reaches of the YRV (Fig. 6e). In MJJ 1998, however, the meridional gradient of the atmospheric circulation over mid and high latitudes was larger than that in 2016, since the Ural high ridge and the trough over

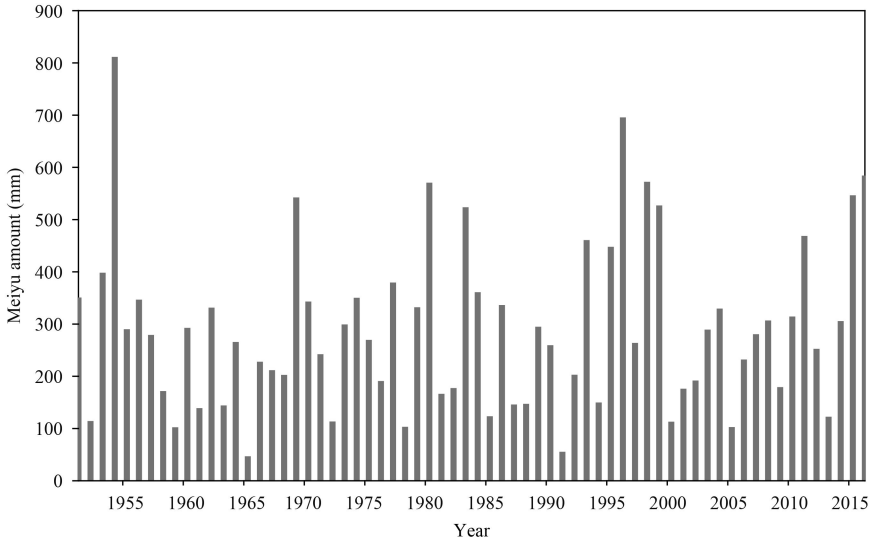

Fig. 5. Annual Meiyu amount (mm) over the mid and lower reaches of the Yangtze River from 1951 to 2016.

Lake Baikal were both stronger than normal (Fig. 6b). Nevertheless, the circulation anomalies of the subtropical region in 1998 were similar to those in 2016. The WPSH was stronger than normal and its high ridge also extended more westward. The anomalous low-level anticyclone also controlled the western Pacific (Fig. 6d) and resulted in anomalous moisture convergence in the YRV (Fig. 6f). Meanwhile, slight differences can also be discerned between 1998 and 2016. The high ridge of the WPSH extended to 110°E in MJJ 2016, which was slightly eastward compared to that in 1998 (100°E). The intensity of the WPSH was a little stronger in 2016 than that in 1998; and in this regard, is ranked third since 1950, behind 2010 and 2015. The PSAC was situated a little farther north and west in 2016 than that in 1998, and had greater strength in 1998. The anomalous convergence center of moisture flux over the mid and lower reaches of the YRV was smaller in 2016 than that in 1998, with its intensity weaker in 2016.

In August 2016, a significant turning occurred in the atmospheric circulation pattern. The meridional gradient became larger, with the Ural high ridge becoming stronger than normal. The WPSH fractured into two parts. The eastern part retreated eastward, and the western part combined with the continental high and controlled eastern China (Fig. 7a). Negative anomalies of

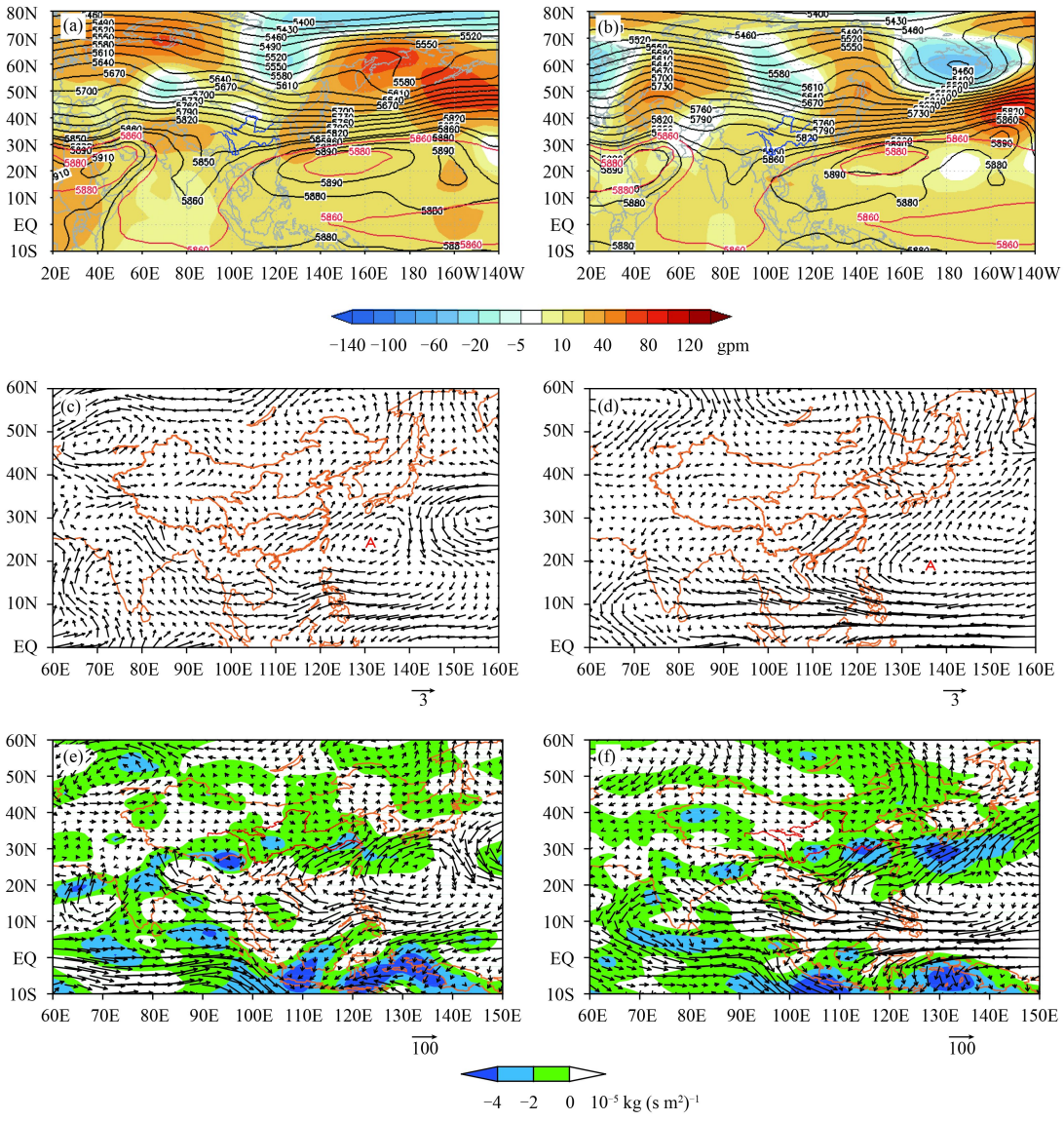

Fig. 6. General circulation fields in MJJ (a, c, e) 2016 and (b, d, f) 1998: (a, b) 500-hPa geopotential height (contours) and anomalies (shading), in which the red contours are the climatological 5860- and 5880-gpm contours; (c, d) 850-hPa horizontal wind anomalies, in which "A" indicates the anomalous anticyclone center (m s^{-1}); (e, f) anomalous moisture flux vertically integrated from 1000 to 300 hPa [vectors; kg (m s)$^{-1}$] and anomalous moisture flux divergence [shading; 10^{-5} kg (s m^2)$^{-1}$].

500-hPa geopotential height dominated over northwestern Pacific, and the low-level circulation also changed from an anticyclonic to a cyclonic anomaly (Fig. 7c). Accordingly, the water vapor transport became weaker and anomalous divergence of moisture flux dominated over the mid and lower reaches of the YRV (Fig. 7e). In August 1998, the atmospheric circulation at mid and high latitudes was similar to that in 2016. However, the circulation anomaly in subtropical regions was significantly different between 1998 and 2016. The WPSH in August 1998 was persistently stronger than normal, with its high ridge also extending more westward (Fig. 7b). The anomalous low-level PSAC continuously dominated over western Pacific (Fig. 7d) and caused anomalous convergence of moisture flux in the middle reaches of the YRV (Fig. 7f). All these features were similar to the conditions in the previous MJJ of 1998.

Therefore, the intraseasonal variation was more significant in the summer of 2016 than in the summer of 1998. During 2016, the meridional gradient of atmospheric circulation at mid and high latitudes became larger in August than in MJJ, with the Ural high ridge becoming stronger in August. The WPSH also showed significant change from MJJ to August. It was stronger than normal and extended more westward in MJJ, but fractured in August. On the contrary, only slight change could be observed in the circulation anomaly at mid and high latitudes in 1998, and the WPSH was persistently intensified from May to August in 1998. The daily variation of 500-hPa geopotential height averaged within 40°–60°N shows similar results. The Ural high was mostly weak in MJJ 2016, but turned to be strong in August. However, the Ural high was strong in MJJ 1998, and then the high over Lake Baikal became intensified in

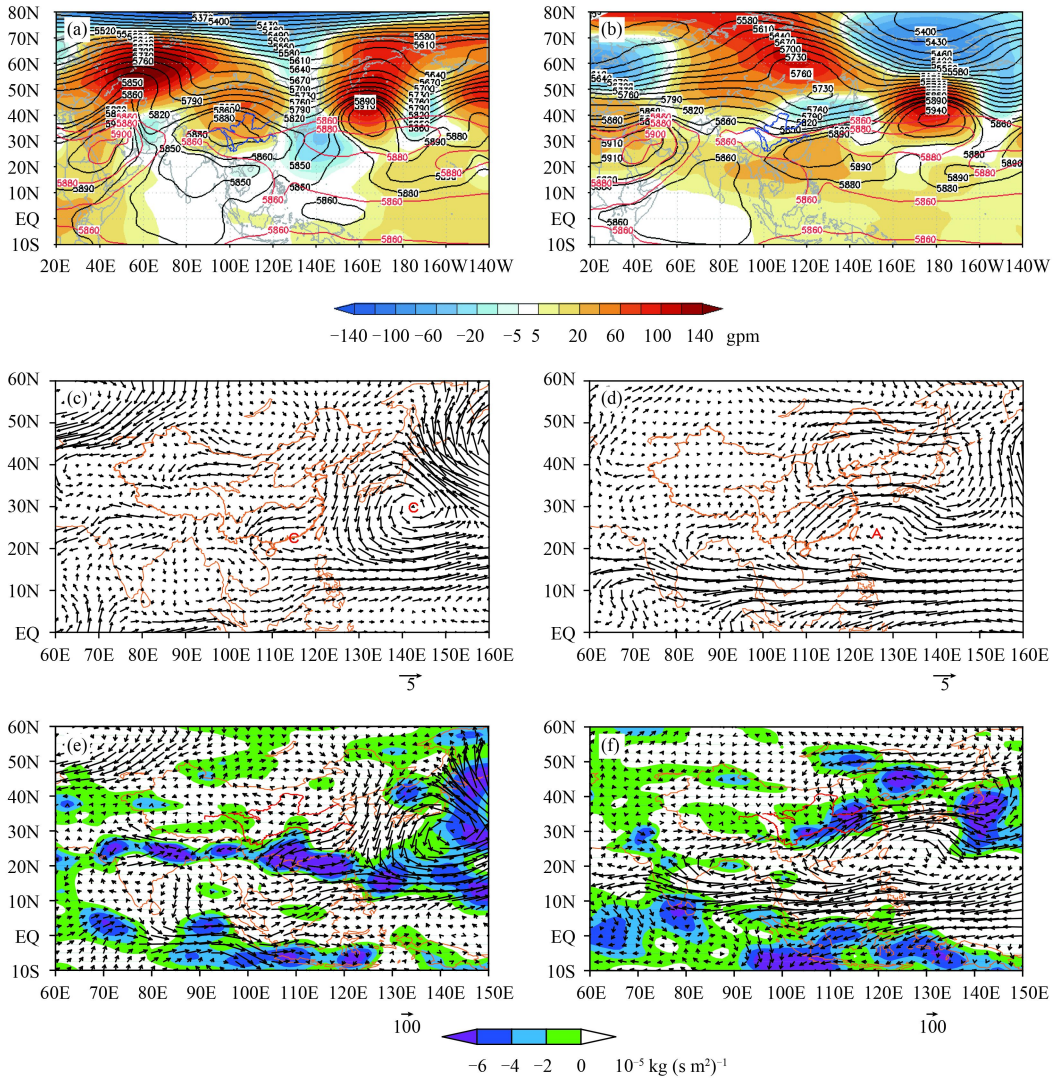

Fig. 7. As in Fig. 6, but for the circulation fields in August, and the character "C" indicates the anomalous cyclone center.

August (Fig. 8a).

4.2 *EASM*

In 2016, the SCSSM broke out in the fifth pentad of May (21–25 May), with its intensity weaker than normal. This feature was similar to 1998; the SCSSM broke out in the fourth pentad of May (16–20 May), and it was also weaker than normal. However, the process and evolution of the EASM showed some differences between the two years. In 2016, the tropical summer monsoon established later than normal. In particular, the convection over the Bay of Bengal (BOB) and Indochina Peninsular was inactive, and the summer monsoon broke out about 2–3 pentads later than normal. During the evolution of the EASM and South Asian summer monsoon, there was convective propagation from north to south, and also from south to north. During the outbreak phase of the EASM, the cold air activities also played an important role. In 1998, however, the EASM established about 3–5 pentads earlier in regions from eastern India to the western BOB, southwestern South China Sea and western Indochina Peninsular; and about 3–5 pentads later in Northwest India, east of Pakistan, western Pacific, Philippines, and eastern Taiwan.

Daily monitoring of the EASM index shows that the EASM was weaker than normal during MJJ of 2016 and 1998. In this period, not only was the daily variation of the monsoon intensity similar, but also, the intraseasonal variation of its phase mostly coincided between the two years. However, the two monsoon indices showed significantly opposite variation from later July and the end of August. The EASM became stronger in 2016, while it was persistently weaker in 1998, and even weaker than that in MJJ (Fig. 8b). Daily monitoring of the PSAC index also shows that it was mostly positive during MJJ of 2016 and 1998, indicating an anomalous anticyclone in northwestern Pacific. However, the PSAC was a little weaker in 2016 than in 1998. The significant turning also occurred in later July, with large negative values in 2016 and still positive values in 1998 (Fig. 8c). This feature indicates that the anomalous anticyclone suddenly changed to a cyclone over northwestern Pacific in 2016. The sig-

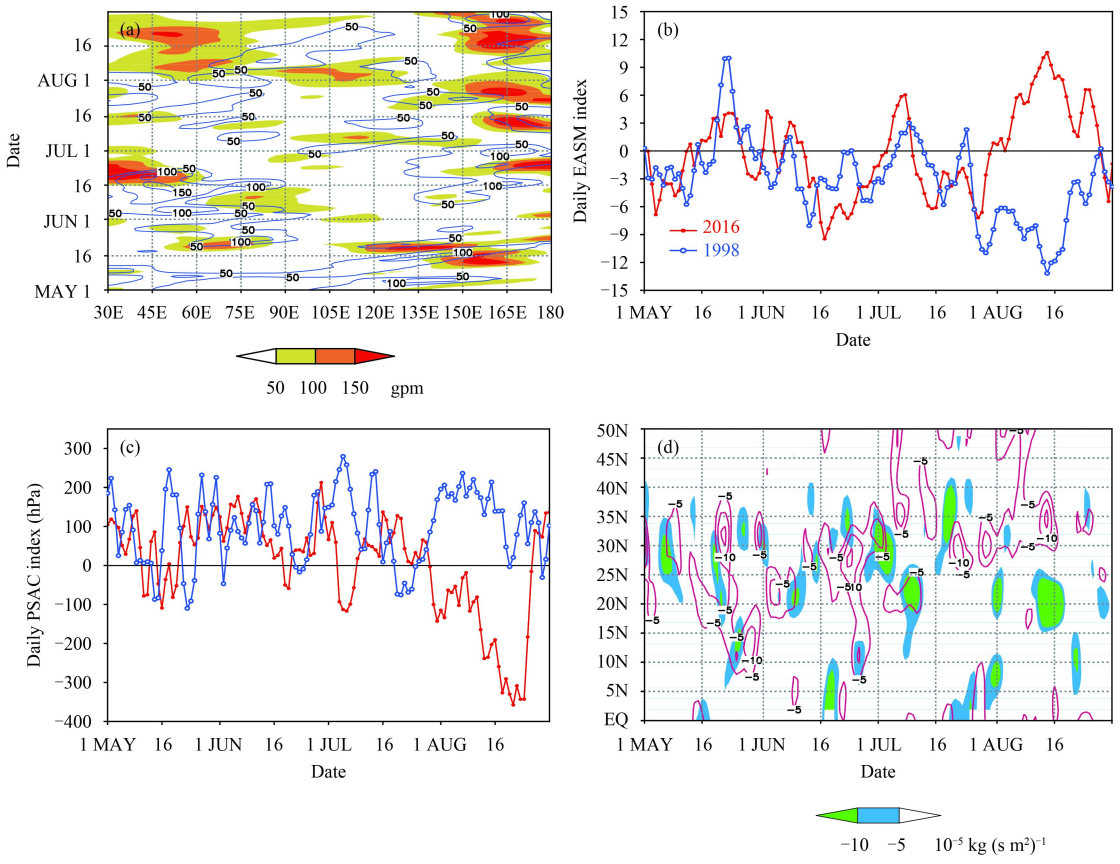

Fig. 8. (a) Time–longitude cross-sections of 500-hPa geopotential height averaged over 40°–60°N from 1 May to 31 August (contours for 1998 and shading for 2016; gpm). (b) Daily East Asian summer monsoon index (red for 2016, blue for 1998; m s^{-1}). (c) Daily Philippine Sea anticyclone index (red for 2016, blue for 1998; hPa). (d) Moisture flux divergence anomalies averaged over 110°–120°E [contours for 1998 and shading for 2016; 10^{-5} kg $(s\ m^2)^{-1}$].

nificant turning of the subtropical atmospheric circulation also led to change of the tropical water vapor transport. From May to mid-July 2016, the anomalous convergence of moisture flux was located around 30°N, favoring more precipitation over the YRV. From later July to the end of August, however, the moisture flux suddenly changed to anomalous divergence in the YRV. On the contrary, the anomalous convergence of moisture flux persistently dominated within 30°–35°N from May to August in 1998 (Fig. 8d).

5. External forcing factors

5.1 *Tropical SSTA*

One of the significant common features of the tropical SSTA's evolution between 2016 and 1998 is the super El Niño event (Fig. 9); the summer seasons of both 2016 and 1998 were both in the decaying phase of a super El Niño. The WPSH was stronger than normal and its high ridge extended more westward during the previous winter and spring of both 2016 and 1998 (Li, 1999; Yuan et al., 2016). During MJJ 2016, the WPSH was still intensified, the EASM was weaker than normal, an anomalous low-level anticyclone prevailed over the northwestern Pacific, and tropical moisture flux was stronger than normal. All these subtropical circulation features were similar to those in 1998, which should be considered as the significant responses of the super El Niño event. Aside from El Niño, the evolution of the SSTA in the TIO also displayed similar characteristics in the two years. During the previous winter and spring of 2016 and 1998, a basin-wide warming SSTA mode dominated in the TIO. Moreover, the IOBW index in the winter of 2015/16 was larger than that in 1997/98, and ranked first since 1950 (Yuan et al., 2016). The IOBW mode mainly exhibited as a lagged response to the El Niño event. However, it acted as a "capacitor" and played an important role in maintaining the impact of El Niño in East Asia during its decaying seasons (Wu and Kirtman, 2004; Annamalai et al., 2005; Yang et al., 2007; Yuan et al., 2008, 2012; Xie et al., 2009). During the developing autumn and winter of El Niño, it usually excites an anomalous low-level anticyclone around the Philippines through the Rossby wave teleconnection. This PSAC is also regarded as an important link for the influence of El Niño on the East Asian climate (Zhang et al., 1999; Wang et al., 2000; Wang and Zhang, 2002). Therefore, during the autumn and winter of El Niño years, the WPSH will intensify and extend more westward and southward, causing more moisture flux from western Pacific to southern China, thereby leading to more precipitation in that region (Zhou and Wu, 2010; Zhou et al., 2010; Zhou, 2011; Yuan et al., 2014a). However, during the decaying summer of El Niño, the warming SSTA weakens over the equatorial eastern–central Pacific. Then, the intensified WPSH during that time is mostly influenced by the persistent warming in the TIO (Xie et al., 2009; Yuan et al., 2012). Considering the warming trend of the SSTA in the TIO and of the subtropical atmospheric circulation (Hu et al., 2003), the linear trend of the IOBW index and the intensity index of the WPSH was removed before correlation analysis. It shows that the monthly correlation coefficients of the WPSH from May to August with February–April mean IOBW and Niño3.4 are above the 95% confidence level. However, during most months, the correlation with IOBW is a little larger than that with Niño3.4 (Fig. 10a), indicating that the effect of the Indian Ocean SSTA would be stronger than the El Niño event during the decaying months of El Niño. Monthly correlation coefficients between the WPSH and IOBW, and between the WPSH and Niño3.4, also show the persistent and significant influence of the SSTA in the TIO and the weakening impact of El Niño (Fig. 10b). It is further confirmed that the Indian Ocean SSTA plays a more important role in the intensified WPSH during the decaying summer of El Niño. Therefore, the exceptional warming mode of the TIO was one of the important external-forcing factors for the anomalous feature of subtropical atmospheric circulation during MJJ 2016, which was similar to that in MJJ 1998.

5.2 *SSTA NAT mode*

In the North Atlantic Ocean, the seasonal–decadal variation of the SSTA is mainly influenced by the North Atlantic Oscillation, ENSO, and decadal variability (Hu Z. Z. et al., 2011). Since the North Atlantic Ocean is located in the mid and high latitudes, its SSTA is mostly influenced by atmospheric forcing, and its response to the atmosphere is very limited. However, recent studies have also indicated that the SSTA NAT mode in the previous winter and spring shows significant impacts on the atmospheric circulation anomaly at mid and high latitudes over Eurasia during the following summer (Wu et al., 2009; Zuo et al., 2012, 2013). A positive (negative) triple mode in spring will result in a weak (strong) Ural high ridge in summer through exciting a Rossby wave. During the previous winter and spring of 2016, the triple mode was persistently positive, and was strong in March and April (Fig. 11a). This was totally different from 1998, when the negative triple mode continued from the previous winter until the following summer (Fig. 11a).

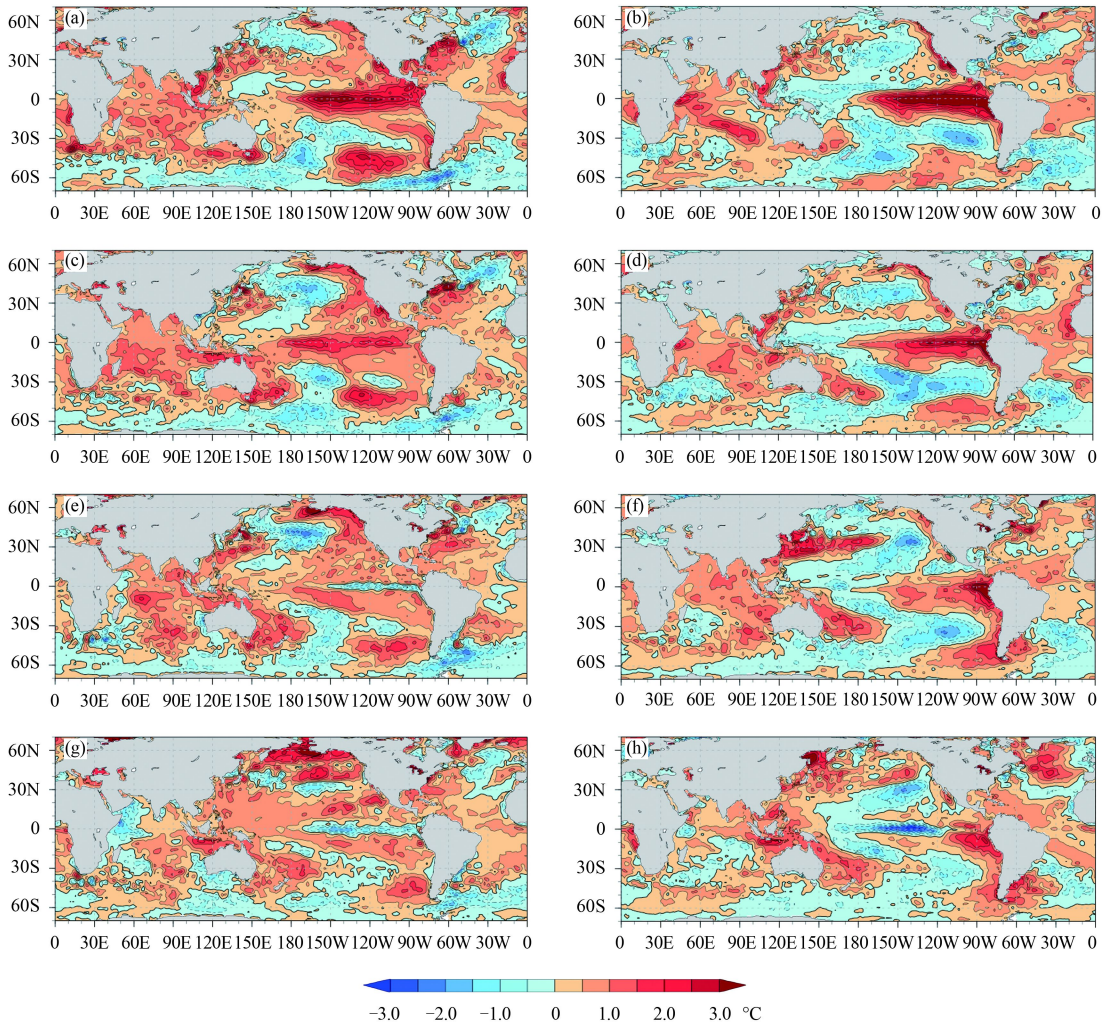

Fig. 9. Monthly mean SST anomaly in (a, c, e, g) 2016 and (b, d, f, h) 1998: (a, b) January, (c, d) March, (e, f) May, and (g, h) July.

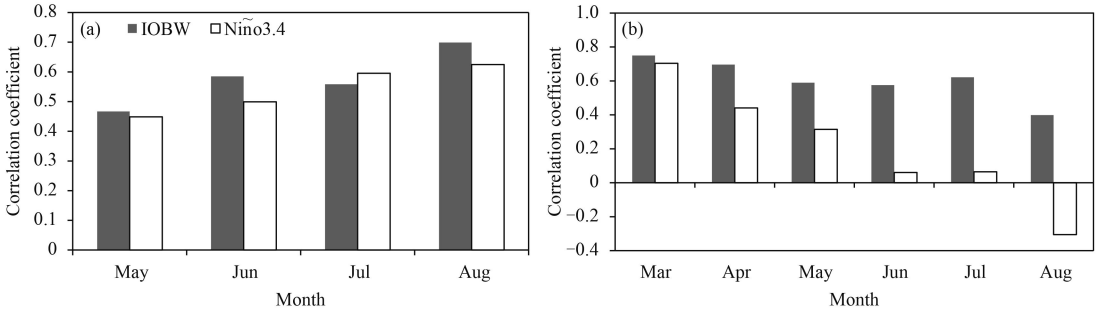

Fig. 10. (a) Correlation coefficients (CCs) of monthly WPSH intensity (WPSHI) from May to August with the IOBW index (grey column) and Niño3.4 index (white column) averaged for February–April of 1980–2015, respectively. (b) Monthly CCs of WPSHI with simultaneous IOBW and Niño3.4 indices from March to August. The linear trends of the IOBW index and WPSHI were removed before correlation analysis.

The correlation map between the February–April mean NAT and the MJJ 500-hPa geopotential height shows that there were "– + – + –" related regions from the North Atlantic Ocean to East Asia via Europe. The negative correlation around the Ural mountains (60°E) was significant (Fig. 11b), indicating that when the NAT is in a negative phase in the previous spring, the Ural high ridge will be stronger than normal in summer, and vice versa. During February–April 1998, a strong negative NAT mode caused the Ural high ridge to be stronger than normal in MJJ. However, during that time in 2016, the NAT was positive, and the Ural high ridge was weaker

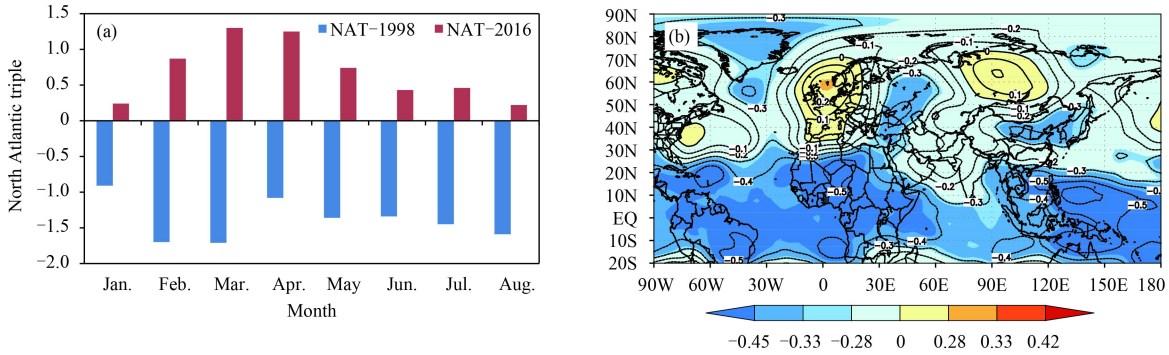

Fig. 11. (a) Monthly NAT (North Atlantic triple) from January to August (red for 2016, blue for 1998). (b) Correlation coefficients (CCs) between the NAT for February–April and 500-hPa geopotential height for May–July during 1980–2014 (shadings from light to dark are for the CCs above the 90%, 95%, and 99% confidence levels, respectively, based on the Student's *t* test).

than normal in MJJ, consistent with the statistical result. Therefore, the different phases of the NAT mode likely contributed to the different circulation anomalies at mid and high latitudes in MJJ between 1998 and 2016.

5.3 *Snow cover over the QTP*

Because of its special geographical location and terrain height characteristics, as well as its significant seasonal and interannual variability as a heat source, the QTP plays an essential role in the formation and anomalies of the East Asian monsoon climate. The snow cover on the QTP is a very important factor reflecting the heat conditions of the plateau, and is one of the important external-forcing factors for the diagnosis and prediction of droughts and floods in the summer season in China (Chen and Song, 2000; Chen et al., 2000; Peng et al., 2005). Previous studies have indicated that the snow cover over the QTP influences the atmospheric circulation in East Asia and further influences the strength of the EASM and summer precipitation over the YRV. More (less) snow cover over the QTP will result in more (less) summer precipitation over the YRV (Zhang and Tao, 2001). One of the important external-forcing factors for the persistent flooding in the YRV in 1998 was the exceptionally large snow cover area over the plateau during the previous winter (Li, 1999). In the winter of 1997/98, a rare snow disaster occurred in the QTP, and the snow cover was still larger than normal in the following spring. According to the theoretical study of radiation and snow feedback effects, larger areas of snow cover will increase the albedo of the snow surface and, thus, the reflection of solar radiation. As a result, the plateau will receive less solar radiation, and the thermal effect of the plateau will also be weakened. The reduced Asian summer monsoon caused by the sea–land heat differences will thereby lead to the southward movement of the main summer rainfall belt (Li, 1999). During the winter of 2015/16, the area of snow cover was also larger than normal, but relatively smaller than that in 1997/98 (Fig. 12a). Moreover, the depth of the winter snow cover was shallower than normal in the winter of 2015/16 based on satellite observations, but deeper than normal in the winter of 1997/98 (Fig. 12a). From the previous winter to spring of 2016, the snow cover changed from more than normal to less than normal. On the contrary, the area of snow cover was persistently larger than

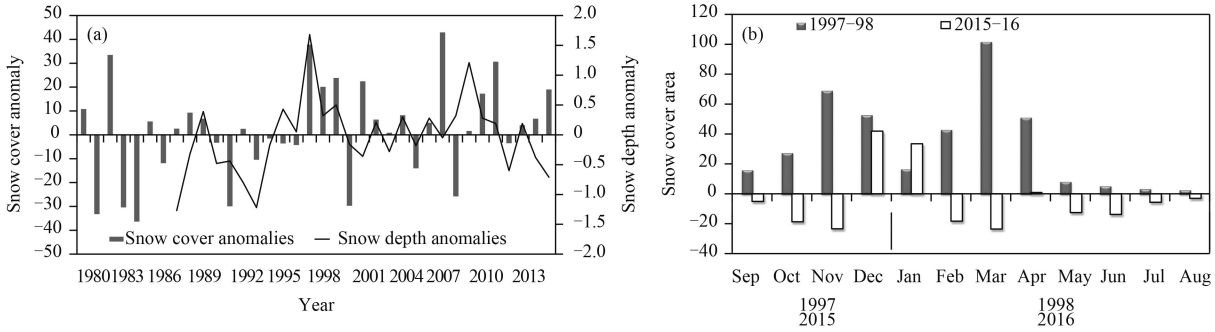

Fig. 12. (a) Snow cover anomalies (bars; 10^5 km^2; left-hand axis) and snow depth anomalies (line; cm; right-hand axis) averaged over the QTP (26°–40°N, 74°–104°E) in the winter during 1980–2015. (b) Monthly snow cover areas averaged over the QTP from September 1997 to August 1998 (grey bars) and from September 2015 to August 2016 (white bars).

normal from the previous winter to spring of 1998 (Fig. 12b). This means that the sensible heat effect of snow cover over the QTP was weaker in 2016 than in 1998, and the persistence of snow cover in 2016 was not so strong as that in 1998. The larger area of snow cover over the TP in the previous winter excited an anomalous low-level anticyclone over northwestern Pacific in the following summer (figure omitted). Plus, the correlation coefficient between the snow cover area index and the EASM index during 1980–2015 was –0.37, significant above the 95% confidence level. Therefore, the relatively weaker sensible heat effect in the previous winter of 2016 was likely one of the reasons for the relatively stronger summer monsoon and weaker flood in the YRV in 2016, as compared with 1998.

6. MJO

As described in previous sections, a significant turning occurred in the tropical and subtropical atmospheric circulation in August 2016. The WPSH fractured into two parts, and negative anomalies of 500-hPa geopotential height dominated over northwestern Pacific (Fig. 7a). Meanwhile, tropical cyclone activities also became elevated in August 2016, with seven typhoons generated and two landing in South China. Therefore, the fracturing of the WPSH and the negative anomalies of 500-hPa geopotential height were likely related to the strong typhoon activity in northwestern Pacific. But what caused the strong typhoon activities? Analysis indicates that, apart from the exceptionally warm SSTA in the underlying surface, active tropical intraseasonal oscillation, i.e., the MJO, played an important role. In August 2016, an intensified MJO transferred eastward to western Pacific (Phases 6 and 7), and stayed there for over 20 days (Fig. 13a). In August 1998, the MJO was also active; however, it stayed in western Indian Ocean (Phases 1 and 2) (Fig. 13b). It has been presented that different phases of the MJO have different modulating effects on the typhoon activities in northwestern Pacific. Furthermore, the genesis number of typhoons when the MJO is in Phases 6 and 7 tends to be double that when the MJO is in Phases 1 and 2 (Pan et al., 2010). In August 2016, the MJO stayed in Phases 6 and 7 for 25 days, which was about 18 days more than normal (7.4 days) and was the second longest since 1979 (Fig. 14a). Meanwhile, the average intensity of the MJO in Phases 6 and 7 was also stronger than normal—the strongest since 2003 (Fig. 14b). On the contrary, the MJO stayed in Phases 6 and 7 for only 2 days in August 1998, with its average intensity weaker than normal. During the decaying August of all moderate and strong El Niño events in history, the duration of the MJO remaining in Phases 6–7 was mostly less than normal, and its strength was mostly weaker than normal. Therefore, the anomalous activities of the MJO in August 2016 acted as one of the important factors for the significant turning of the tropical and subtropical atmospheric circulation anomalies.

Previous studies have reported that the TIO SSTA dipole (IOD) mode significantly influences the eastward propagation of the MJO. The positive phase of the IOD may weaken the eastward propagation of the MJO and

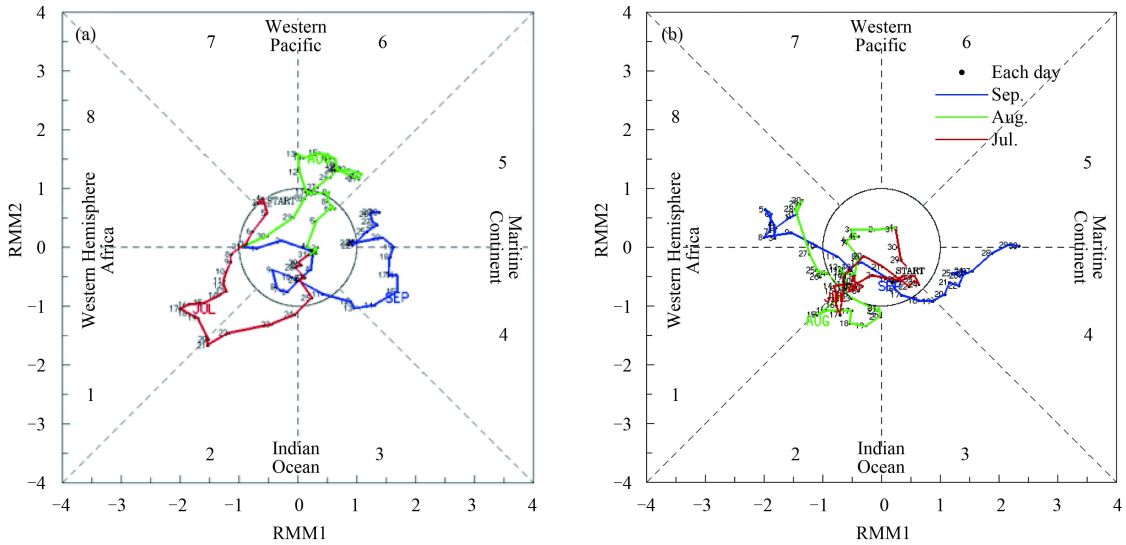

Fig. 13. Madden–Julian Oscillation phase diagrams in July–September for (a) 2016 and (b) 1998. Realtime multivariate MJO index (RMM1 and RMM2) are the two components of MJO index. Source: http://www.bom.gov.au/climate/mjo/. Red, green, and blue one for July, August, and September, respectively.

cause the MJO to be interrupted in eastern Indian Ocean and western Pacific. However, when the IOD is negative, the anomalously warm SSTA in the eastern Indian Ocean and the intensified low-level westerly wind over the central Indian Ocean favor the persistent eastward propagation of the MJO (Yuan et al., 2014b). The MJO will become more active in western Pacific. Before the spring of 2016, the distribution pattern of the SSTA in the TIO–Pacific Ocean was similar to that in 1998 (Fig. 9). However, the cold SSTA began to develop in the equatorial eastern-central Pacific and western Indian Ocean from May 2016 (Fig. 9e). The negative phase of the IOD (with a positive SSTA in the equatorial southeastern Indian Ocean and negative SSTA in western Indian Ocean) became more significant in July 2016 (Fig. 9g). However, the decline of the SSTA in western Indian Ocean in 1998 was not so large as that in 2016, and anomalously warm conditions still dominated over most parts of the Indian Ocean in July 1998 (Fig. 9h). The monthly variation of the IOBW and IOD indices also shows that the positive IOBW in January–April 2016 was stronger than that in 1998, and the negative IOD developed much faster in June–July 2016 than that in 1998 (Fig. 15a). The June–July mean IOD index was –0.96°C in 2016, which was below two standard deviations of this index and ranked the strongest negative one since 1980 (Fig. 15b). During 1980–2016, the correlation coefficient between the June–July mean IOD index and the duration of the MJO in Phases 6–7 in August was –0.42, significant above the 99% confidence level. Therefore, it can be inferred that the rapid development and exceptionally strong negative IOD mode in 2016 was likely responsible for the active MJO and frequent typhoon activities in August 2016.

7. Conclusions and discussion

The precipitation anomaly features in the summer season (MJJA) of 2016 and their differences with 1998 have been analyzed in great detail in this study. The associated atmospheric circulation anomaly and possible external-forcing factors have also been examined and compared. During the summer of 2016, precipitation over most of China was above normal. The summer precipitation averaged over China was 8% above normal and ranked the fourth largest since 1951. There were two

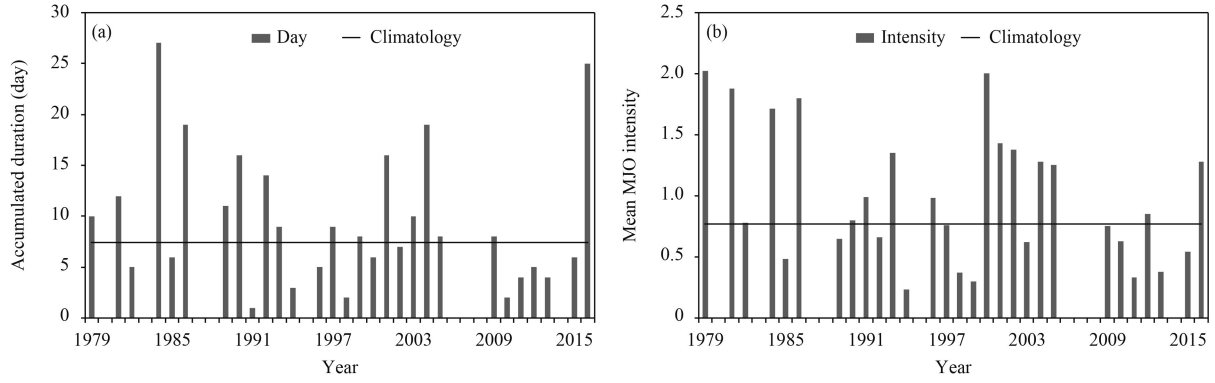

Fig. 14. (a) Accumulated duration (day) and (b) mean intensity of the MJO in Phases 6 and 7 in August from 1979 to 2016.

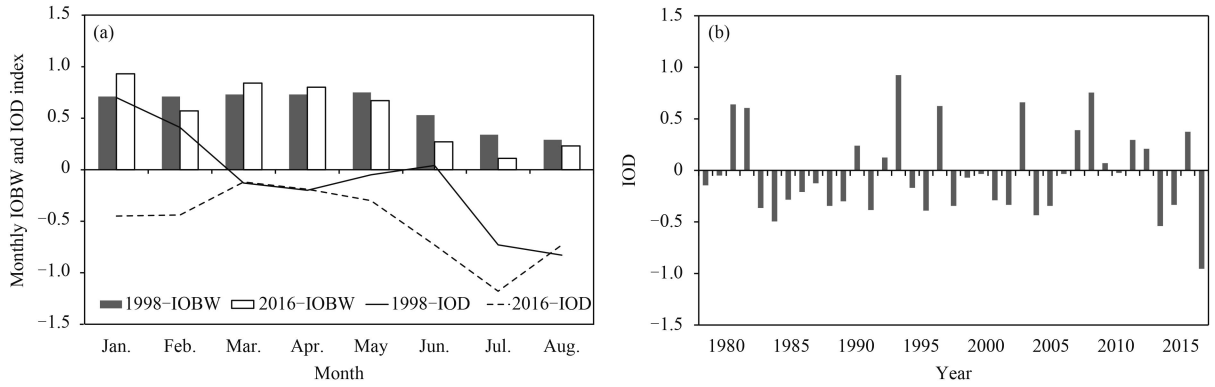

Fig. 15. (a) Monthly Indian Ocean basin-wide (IOBW) and Indian Ocean Dipole (IOD) indices (°C) from January to August in 1998 and 2016. (b) Annual variation of the IOD (°C) averaged in June–July from 1980 to 2016.

main anomalous rainfall belts in eastern China—one in the YRV and the other in northern China. The anomalously high precipitation over the YRV was similar to 1998, but weaker than 1998 and the area smaller. After the end of the Meiyu on 21 July, the precipitation changed to significantly below normal over the YRV until the end of August. However, a "Secondary Meiyu" occurred in 1998 and the precipitation over the YRV was still above normal in August 1998.

Considering the significant turning of the precipitation anomaly in the YRV in August 2016, the atmospheric circulation anomalies averaged in MJJ and August were analyzed separately. During MJJ 2016, the Ural high ridge was weaker than normal and the blocking over the Okhotsk Sea was stronger than normal. During MJJ 1998, however, the Ural high ridge was stronger than normal, resulting in a larger meridional gradient than that in 2016. In the tropical and subtropical regions, the weakened EASM was similar in both 1998 and 2016, and the WPSH was both intensified and extended more westward. Therefore, the anomalous convergence of moisture flux was located in the YRV in both years, causing the similar above-normal precipitation over the mid and lower reaches of the YRV. However, the summer monsoon circulation and rainfall pattern became opposite in August, with dry conditions and high temperatures in the YRV in 2016 and a "Secondary Meiyu" in 1998.

The similar tropical and subtropical atmospheric circulation anomalies during MJJ of 1998 and 2016 can be attributed to the similar SSTA pattern in the tropical ocean, with a typical El Niño event in the previous winter and a basin-wide warming SSTA in the TIO in the following spring. Meanwhile, the Indian Ocean warming mode was strongest in 2016, which would have been one of the important reasons for the relatively stronger WPSH in 2016 than in 1998 during MJJ. For the different atmospheric circulations at mid and high latitudes between the two years, different phases of the NAT likely played an important role. The positive phase of the NAT dominated in the North Atlantic Ocean from the previous winter to the spring of 2016, whereas a negative NAT persisted in 1998. Through exciting a Eurasian teleconnection wave train, the positive (negative) NAT resulted in a weaker (stronger) Ural high ridge in 2016 (1998). The area of snow cover over the QTP in the winter of 2015/16 was smaller than that of 1997/98, and its depth was also shallower in 2015/16 than in 1997/98. Combined with the weaker persistence of the snow cover anomaly in 2016, the relatively weaker thermal effect of the snow cover on the QTP may have led to a slightly stronger EASM and slightly less summer precipitation in the YRV in 2016, as compared with 1998.

The significant change of the subtropical atmospheric circulation in August 2016 was related to abnormal MJO activities. In August 2016, the MJO was persistently stronger than normal and it stayed in western Pacific (Phases 6–7) for 25 days—the second longest since 1979. However, the MJO stayed in Phases 6–7 for only 2 days in August 1998, and its intensity was largely weaker than normal. During the decaying August of most moderate and strong El Niño events in history, the duration of the MJO in Phases 6–7 has mostly been less than normal. In August 2016, the active MJO excited frequent typhoon activities, which in turn influenced the strength and pattern of the WPSH. As a result, the WPSH fractured, and a negative anomaly of 500-hPa geopotential height dominated over northwestern Pacific. Further analysis indicated that the rapid development of the abnormally strong negative phase of the IOD was probably an important reason for the strong MJO activity in August 2016.

It should be emphasized that all these external-forcing signals, such as the tropical SSTA, NAT, and snow cover on the QTP, are all important factors influencing summer precipitation in China. These factors showed significant anomalies in 2016 and became leading factors for summer precipitation in China. Therefore, they displayed significant correlations with the summer precipitation in 2016. However, this does not mean that all these signals will still be significant during other years, because the climate impact of the external-forcing factors is dominated by the anomalies of these factors themselves. On the other hand, studies of multi-factor interaction are still quite preliminary, and the nonlinear effects of the internal dynamics of the atmosphere itself are very important. Both the external forcing and the integrated effect within the atmosphere restrict the summer climate in China, especially the position and amounts of the main rainfall belt. For example, Wang (2005) found that the persistence of the atmospheric anomalies determined by the internal variation of the atmosphere leads to partial predictability of the East Asian monsoon climate, and the link is the global circulation changes associated with the East Asian monsoon. Zhang et al. (2007) pointed out that, different from the precipitation in eastern China influenced by ocean forcing, the decadal variation of the summer precipitation in Northwest China is closely related to the internal dynamic processes of atmospheric circulation, i.e., the disturbed kinetic energy of westerlies at midlatitudes in Asia. In the last 10 years, studies have also revealed the important contribution of the previous circulation anomaly signals of the Southern Hemisphere to the EASM, and to summer precipitation predic-

tion in China. For the atmospheric circulation anomalies at mid and high latitudes particularly, the impact of external forcing factors is very limited. Most of the precipitation change is the climate noise of internal dynamics (Si et al., 2016). However, the present study's aim was to compare the difference in summer precipitation between 2016 and 1998. The above internal dynamic processes of circulation and the associated prediction information were not examined. On the other hand, this study mainly analyzed the summer precipitation anomaly in southern China. Our understanding of the mechanism of flood and drought distributions over northern China in 2016 still needs to be improved. Summer precipitation in Northeast China also showed different features between 1998 and 2016. More precipitation occurred in Northeast China in May–June 2016, which suddenly changed to dry conditions in July–August. However, precipitation was above normal in each month of the summer in 1998, especially in eastern Inner Mongolia. This might have partly resulted from the trough in the western part of the blocking over the Sea of Okhotsk. Another reason was probably the frequent activities of the cold vortex in Northeast China. More studies are still needed to further examine the precipitation anomaly in Northeast China. As for North China, the extreme heavy rainfall process in later July finally resulted in the above-normal summer precipitation. However, if we remove this process, the summer precipitation is less than normal in North China. Therefore, the impact of the heavy rainfall caused by extreme circulation anomalies on short-term climate prediction still needs more in-depth investigations.

REFERENCES

Annamalai, H., S. P. Xie, J. P. McCreary, et al., 2005: Impact of Indian Ocean sea surface temperature on developing El Niño. *J. Climate*, **18**, 302–319, doi: 10.1175/JCLI-3268.1.

Chang, A. T. C., P. Gloersen, T. Schmugge, et al., 1976: Microwave emission from snow and glacier ice. *J. Glaciol.*, **16**, 23–39, doi: 10.1017/S0022143000031415.

Chang, A. T. C., J. L. Foster, D. K. Hall, et al., 1982: Snow water equivalent estimation by microwave radiometry. *Cold Regions Science and Technology*, **5**, 259–267, doi: 10.1016/0165-232X(82)90019-2.

Che, T., and X. Li, 2005: Spatial distribution and temporal variation of snow water resources in China during 1993–2002. *Journal of Glaciology and Geocryology*, **27**, 64–67. (in Chinese)

Chen, L. J., Y. Yuan, M. Z. Yang, et al., 2013: A review of physical mechanisms of the global SSTA impact on EASM. *J. Appl. Meteor. Sci.*, **24**, 521–532. (in Chinese)

Chen, L. T., 2001: The role of the anomalous snow cover over the Qinghai–Xizang plateau and ENSO in the great floods of 1998 in the Changjiang River valley. *Chinese J. Atmos. Sci.*, **25**, 184–192. (in Chinese)

Chen, Q. J., B. Gao, W. J. Li, et al., 2000: Studies on relationships among snow cover winter over the Tibetan Plateau and droughts/floods during Meiyu season in the mid and lower reaches of the Yangtze River as well as atmosphere/ocean. *Acta Meteor. Sinica*, **58**, 582–595. (in Chinese)

Chen, X. F., and W. L. Song, 2000: Analysis of relationship between snow cover on Eurasia and Qinghai–Xizang Plateau in winter and summer rainfall in China and application to prediction. *Plateau Meteor.*, **19**, 214–223. (in Chinese)

Chen, X. F., and Z. G. Zhao, 2000: *Study on Precipitation Forecast in China during Flood Season and its Applications*. China Meteorological Press, Beijing. 241 pp. (in Chinese)

Hu, K. M., G. Huang, and R. H. Huang, 2011: The impact of tropical Indian Ocean variability on summer surface air temperature in China. *J. Climate*, **24**, 5365–5377, doi: 10.1175/2011JCLI4152.1.

Hu, Z. Z., S. Yang, and R. G. Wu, 2003: Long-term climate variations in China and global warming signals. *J. Geophys. Res.*, **108**, 4614, doi: 10.1029/2003JD003651.

Hu, Z. Z., A. Kumar, B. H. Huang, et al., 2011: Persistent atmospheric and oceanic anomalies in the North Atlantic from Summer 2009 to Summer 2010. *J. Climate*, **24**, 5812–5830, doi: 10.1175/2011JCLI4213.1.

Kalnay, E., M. Kanamitsu, R. Kistler, et al., 1996: The NCEP/NCAR 40-yr reanalysis project. *Bull. Amer. Meteor. Soc.*, **77**, 437–471, doi: 10.1175/1520-0477(1996)077<0437:TNYRP>2.0.CO;2.

Kistler, R., W. Collins, S. Saha, et al., 2001: The NCEP–NCAR 50-yr reanalysis: Monthly means CD-ROM and documentation. *Bull. Amer. Meteor. Soc.*, **82**, 247–268, doi: 10.1175/1520-0477(2001)082<0247:TNNYRM>2.3.CO;2.

Klein, S. A., B. J. Soden, and N.-C. Lau, 1999: Remote sea surface temperature variations during ENSO: Evidence for a tropical atmospheric bridge. *J. Climate*, **12**, 917–932, doi: 10.1175/1520-0442(1999)012<0917:RSSTVD>2.0.CO;2.

Lau, N. C., and M. J. Nath, 2000: Impact of ENSO on the variability of the Asian–Australian monsoons as simulated in GCM experiments. *J. Climate*, **13**, 4287–4309, doi: 10.1175/1520-0442(2000)013<4287:IOEOTV>2.0.CO;2.

Li, C. Y., R. H. Huang, J. H. Chou, et al., 2009: *The Study of Meteorological Disasters and Chinese Response*. China Meteorological Press, Beijing. 187 pp. (in Chinese)

Li, W. J., 1999: General atmospheric circulation anomaly in 1998 and their impact on climate anomaly in China. *Meteor. Mon.*, **25**, 20–25. (in Chinese)

Liu, C. Z., and F. Xue, 2010: The decay of El Niño with different intensity. Part II: The decay of the moderate and relatively-weak El Niño. *Chinese J. Geophys.*, **53**, 2564–2573. (in Chinese)

Liu, Y. Y., W. J. Li, W. X. Ai, et al., 2012: Reconstruction and application of the monthly western Pacific subtropical high indices. *J. Appl. Meteor. Sci.*, **23**, 414–423. (in Chinese)

Luo, S. H., Z. H. Jin, and L. T. Chen, 1985: The analysis of correlation between sea surface temperature in the Indian–South China Sea and precipitation in the mid and lower reaches of the Changjiang River. *Scientia Atmospherica Sinica*, **9**, 314–320. (in Chinese)

Meyers, G., 1996: Variation of Indonesian throughflow and the El Niño–Southern Oscillation. *J. Geophys. Res.*, **101**, 12255–12263, doi: 10.1029/95JC03729.

National Climate Center, 1998: *China's 1998 Severe Flood and Climate Extremes*. China Meteorological Press, Beijing, 152 pp. (in Chinese)

Pan, J., C. Y. Li, and J. Song, 2010: The modulation of Madden–Julian Oscillation on typhoons in the northwestern Pacific Ocean. *Chinese J. Atmos. Sci.*, **34**, 1059–1070. (in

Chinese)
Peng, J. B., L. T. Chen, and Q. Y. Zhang, 2005: Multi-scale variations of snow cover over QXP and tropical pacific SST and their influences on summer rainfall in China. *Plateau Meteor.*, **24**, 366–377. (in Chinese)
Ren, Z. H., Y. Yu, F. L. Zou, et al., 2012: Quality detection of surface historical basic meteorological data. *J. Appl. Meteor. Sci.*, **23**, 739–747. (in Chinese)
Reynolds, R. W., N. A. Rayner, T. M. Smith, et al., 2002: An improved in situ and satellite SST analysis for climate. *J. Climate*, **15**, 1609–1625, doi: 10.1175/1520-0442(2002)015<1609:AIISAS>2.0.CO;2.
Saji, N. H., B. N. Goswami, P. N. Vinayachandran, et al., 1999: A dipole mode in the tropical Indian Ocean. *Nature*, **401**, 360–363.
Shao, X., and B. Zhou, 2016: Monitoring and diagnosis of the 2015/16 super El Niño event. *Meteor. Mon.*, **42**, 540–547. (in Chinese)
Si, D., Z. Z. Hu, A. Kumar, et al., 2016: Is the interdecadal variation of the summer rainfall over eastern China associated with SST. *Climate Dyn.*, **46**, 135–146, doi: 10.1007/s00382-015-2574-5.
Wang, B., and Q. Zhang, 2002: Pacific–East Asian teleconnection. Part II: How the Philippine Sea anomalous anticyclone is established during El Niño development. *J. Climate*, **15**, 3252–3265, doi: 10.1175/1520-0442(2002)015<3252:PEATPI>2.0.CO;2.
Wang, B., R. G. Wu, and X. H. Fu, 2000: Pacific–East Asian teleconnection: How does ENSO affect East Asian climate. *J. Climate*, **13**, 1517–1536, doi: 10.1175/1520-0442(2000)013<1517:PEATHD>2.0.CO;2.
Wang, H. J., 2005: Preliminary research on the inner-atmosphere-originated seasonal climate predictability. *Chinese J. Atmos. Sci.*, **29**, 64–70. (in Chinese)
Wang, Q., S. L. Li, J. J. Fu, et al., 2012: On the formation of anomalous summer precipitation in the years of 2010 and 1998. A comparison of the El Niño's impact between Modoki and typical El Niño cases. *Acta Meteor. Sinica*, **70**, 1207–1222. (in Chinese)
Wheeler, M. C., and H. H. Hendon, 2004: An all-season real-time multivariate MJO index: Development of an index for monitoring and prediction. *Mon. Wea. Rev.*, **132**, 1917–1932, doi: 10.1175/1520-0493(2004)132<1917:AARMMI>2.0.CO;2.
Wu, R. G., and B. P. Kirtman, 2004: Understanding the impacts of the Indian Ocean on ENSO variability in a coupled GCM. *J. Climate*, **17**, 4019–4031, doi: 10.1175/1520-0442(2004)017<4019:UTIOTI>2.0.CO;2.
Wu, Z. W., B. Wang, J. P. Li, et al., 2009: An empirical seasonal prediction model of the East Asian summer monsoon using ENSO and NAO. *J. Geophys. Res.*, **114**, D18120, doi: 10.1029/2009JD011733.
Xie, S. P., K. M. Hu, J. Hafner, et al., 2009: Indian Ocean capacitor effect on Indo–western Pacific climate during the summer following El Niño. *J. Climate*, **22**, 730–747, doi: 10.1175/2008JCLI2544.1.
Xue, F., and C. Z. Liu, 2008: The influence of moderate ENSO on summer rainfall in eastern China and its comparison with strong ENSO. *Chin. Sci. Bull.*, **53**, 791–800, doi: 10.1007/s11434-008-0002-5.
Yang, J. L., Q. Y. Liu, S. P. Xie, et al., 2007: Impact of the Indian Ocean SST basin mode on the Asian summer monsoon. *Geophys. Res. Lett.*, **34**, L02708, doi: 10.1029/2006GL028571.
Yuan, Y., H. Gao, X. L. Jia, et al., 2016: Influences of the 2014–2016 super El Niño event on climate. *Meteor. Mon.*, **42**, 532–539. (in Chinese)
Yuan, Y., W. Zhou, J. C. L. Chan, et al., 2008: Impacts of the basin-wide Indian Ocean SSTA on the South China Sea summer monsoon onset. *Int. J. Climatol.*, **28**, 1579–1587, doi: 10.1002/joc.v28:12.
Yuan, Y., S. Yang, and Z. Q. Zhang, 2012: Different evolutions of the Philippine Sea anticyclone between the eastern and central Pacific El Niño: Possible effects of Indian Ocean SST. *J. Climate*, **25**, 7867–7883, doi: 10.1175/JCLI-D-12-00004.1.
Yuan, Y., C. Y. Li, and S. Yang, 2014a: Decadal anomalies of winter precipitation over southern China in association with El Niño and La Niña. *J. Meteor. Res.*, **28**, 91–110.
Yuan, Y., H. Yang, and C. Y. Li, 2014b: Possible influences of the tropical Indian Ocean dipole on the eastward propagation of MJO. *J. Trop. Meteor.*, **20**, 173–180.
Zhai, P. M., R. Yu, Y. J. Guo, et al., 2016: The strong El Niño in 2015/16 and its dominant impacts on global and China's climate. *J. Meteor. Res.*, **30**, 283–297, doi: 10.1007/s13351-016-6101-3.
Zhang, Q. Y., S. Y. Tao, and L. T. Chen, 2003: The inter-annual variability of East Asian summer monsoon indices and its association with the pattern of general circulation over East Asia. *Acta Meteor. Sinica*, **61**, 559–568. (in Chinese)
Zhang, Q. Y., J. M. Lü, L. M. Yang, et al., 2007: The interdecadal variation of precipitation pattern over China during summer and its relationship with the atmospheric internal dynamic processes and extra-forcing factors. *Chinese J. Atmos. Sci.*, **31**, 1290–1300. (in Chinese)
Zhang, R. H., A. Sumi, and M. Kimoto, 1999: A diagnostic study of the impact of El Niño on the precipitation in China. *Adv. Atmos. Sci.*, **16**, 229–241, doi: 10.1007/BF02973084.
Zhang, S. L., and S. Y. Tao, 2001: Influences of snow cover over the Tibetan Plateau on Asian summer monsoon. *Chinese J. Atmos. Sci.*, **25**, 372–390. (in Chinese)
Zhao, Z. G., 1999: *Summer Drought and Flood in China and the Circulation Patterns*. China Meteorological Press, Beijing, 297 pp. (in Chinese)
Zhou, L. T., 2011: Impact of East Asian winter monsoon on rainfall over southeastern China and its dynamical process. *Int. J. Climatol.*, **31**, 677–686, doi: 10.1002/joc.v31.5.
Zhou, L. T., and R. G. Wu, 2010: Respective impacts of the East Asian winter monsoon and ENSO on winter rainfall in China. *J. Geophys. Res.*, **115**, D02107, doi: 10.1029/2009JD012502.
Zhou, L. T., C. Y. Tam, W. Zhou, et al., 2010: Influence of South China Sea SST and the ENSO on winter rainfall over South China. *Adv. Atmos. Sci.*, **27**, 832–844, doi: 10.1007/s00376-009-9102-7.
Zuo, J. Q., W. J. Li, H. L. Ren, et al., 2012: Change of the relationship between spring NAO and East Asian summer monsoon and its possible mechanism. *Chinese J. Geophys.*, **55**, 384–395. (in Chinese)
Zuo, J. Q., W. J. Li, C. H. Sun, et al., 2013: Impact of the North Atlantic sea surface temperature tripole on the East Asian summer monsoon. *Adv. Atmos. Sci.*, **30**, 1173–1186, doi: 10.1007/s00376-012-2125-5.

Tech & Copy Editor: Xueyan ZHANG
Language Editor: Colin SMITH